ADVANCED ELECTRONIC MATERIALS
www.advelectronicmat.de

Self-Powered High-Detectivity Lateral MoS_2 Schottky Photodetectors for Near-Infrared Operation

*Yichen Mao, Pengpeng Xu, Qiang Wu, Jun Xiong, Renmiao Peng, Wei Huang, Songyan Chen, Zhengyun Wu, and Cheng Li**

2D transition metal dichalcogenides (TMDs) have been widely investigated for possible application in field-effect transistors and optoelectronic devices. However, due to the wide band gap of most TMDs, photoresponse to infrared wavelength is still a big challenge. Here, a lateral molybdenum disulfide (MoS_2)-on-metal Schottky photodetector operating in internal photoemission mode for near-infrared wavelength with high responsivity is reported. With moderate Schottky barrier height, a low dark current of 0.12 nA at −0.5 V and a remarkable rectification ratio of 10^3 at ±0.8 V are realized in the MoS_2-on-Au Schottky photodetector. The maximum responsivity of 1.9 A W^{-1} at −1 V is achieved at 1310 nm due to the photoemission from the underlayering Au electrode, which absorbs most of the incident light through the transparent MoS_2 layers, and the generated photocurrent gain in MoS_2 layers. Furthermore, the MoS_2 Schottky photodetectors are self-powered. The high responsivity of 0.68 A W^{-1} and the excellent specific detectivity of 1.89×10^{12} Jones at 1310 nm are obtained under 0 V. The excellent performance demonstrates that internal photoemission mechanism can be well applied in 2D material Schottky photodetectors for infrared wavelengths.

1. Introduction

2D transition metal dichalcogenides, such as MoS_2, tungsten diselenide, etc., have been widely investigated for their possible application in field-effect transistors and optoelectronic devices.[1–9] Various structures of MoS_2 photodetector including p–n junction, metal-semiconductor-metal, and photoconductor, etc. showed high performance. The multilayer MoS_2 phototransistor with a responsivity of 120 mA W^{-1} and a detectivity of 10^{11} Jones for visible light was designed and fabricated.[10] The remarkable responsivity of 880 A W^{-1} at 561 nm was achieved for a monolayer MoS_2 photoconductor at 8 V bias voltage with ultra-high photocurrent gain.[11] Furthermore, a MoS_2 p–n junction has been realized, showing high responsivity of 107 A W^{-1} at 650 nm and operating at zero bias voltage.[12]

Most of the MoS_2 photodetectors operate in the range of visible spectrum due to interband transition. The band gap of MoS_2 can be tuned from 1.2 to 1.8 eV, according to the number of layers, which determines the photoresponse range in the visible spectrum.[13–15] The limited photoresponse range restricts the application of MoS_2 in the infrared photodetection. Hence, it is essential to extend the response range of MoS_2 photodetectors to near-infrared wavelength. One possible solution is to combine MoS_2 and other narrow band gap materials such as black phosphorous, to fabricate photodetectors operating near-infrared wavelength.[16] The other is to utilize internal photoemission effect of Schottky junctions for infrared light detection.[17,18] Several MoS_2 Schottky photodetectors for infrared light detection have been reported,[19–22] in which, plasmonic antenna array electrodes, vertical MoS_2 Schottky junction, and MoS_2 field-effect transistors were proposed to enhance response to near-infrared wavelength. However, the problem is that the quantum efficiency of the internal photoemission is usually much lower than that of interband transition. It is necessary to further investigate MoS_2 Schottky photodetectors with low dark current and high performance for near-infrared operation in a low-cost fabrication method.

In this work, a lateral MoS_2 Schottky photodetector was proposed and fabricated by firstly transferring multilayer MoS_2 on metal (Au, Ti) to form Schottky contact with a Van der Waals gap and then deposition of Ti on the MoS_2 to form Ohmic contact. Ti deposited on surface of MoS_2 can form covalent bond between S and Ti atoms, rendering good Ohmic contact, as previously reported.[23] Due to the multilayer MoS_2 lying on Au electrode of the Van der Waals contact, the near-infrared light would penetrate through the MoS_2 flakes to be fully absorbed by the metal electrode to excite internal photoemission electrons at the contact interface. In this MoS_2-on-Au Schottky photodetector, a remarkable rectification ratio of 10^3 at ±0.8 V and an excellent dark current of 0.12 nA at −0.5 V bias voltage have been realized. Based on internal photoemission mechanism and the internal electric field formed by the Schottky junction, self-powered photodetection characteristics have been observed in the MoS_2-on-Au Schottky photodetector at near-infrared waveband. This MoS_2-on-Au Schottky photodetector

Y. Mao, P. Xu, Q. Wu, J. Xiong, R. Peng, Dr. W. Huang, Prof. S. Chen, Prof. Z. Wu, Prof. C. Li
Department of Physics
OSED
Semiconductor Photonics Research Center
Xiamen University
Xiamen 361005, China
E-mail: lich@xmu.edu.cn

DOI: 10.1002/aelm.202001138

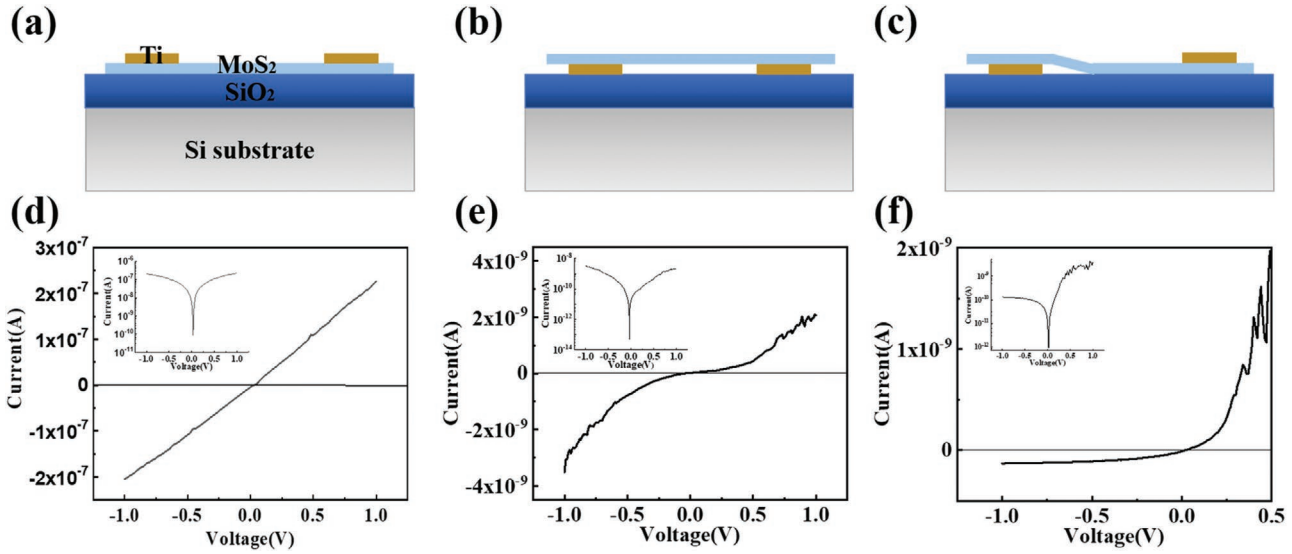

Figure 1. a) The device structure diagram with both Ti electrodes deposited on the surface of MoS2, b) with MoS2 transferred on the surface of both Ti electrodes, c) with one Ti electrodes on and the other below MoS2 layers. d,e) Current–voltage characteristics of the corresponding devices in (a–c), respectively. The insets show the current–voltage characteristics in logarithmic coordinates.

exhibits an outstanding specific detectivity of 1.89×10^{12} Jones at 1310 nm at zero bias voltage due to not only a very low dark current but also a noticeable responsivity of 0.68 A W^{-1}. Finally, a MoS_2-on-Ti Schottky photodetector was also fabricated and exhibited a rectification ratio of 10^2 as well as a responsivity of 66.2 mA W^{-1}. It is demonstrated that this fabrication process to form lateral MoS_2 Schottky junctions might be suitable for other kinds of metals and 2D materials.

2. Results and discussion

In order to demonstrate the different contact properties between MoS_2 and metal formed by different fabrication processes, three kinds of structures of devices were fabricated, as shown in **Figure 1**a–c. Optical images of the corresponding devices are shown in Figure S1, Supporting Information. Here, the electrodes of all devices were made with Ti metal. In Figure 1a, both electrodes were deposited on the surface of MoS_2 by magnetron sputtering. The current depends linearly on voltage and is almost symmetric under positive and negative bias, as shown in Figure 1d, which indicates that ohmic contact has been formed between MoS_2 and Ti. Magnetron sputtering is a kind of high energy deposition technology, which facilitates the formation of covalent bonds between MoS_2 and Ti as well as metallization of MoS_2 contacting with Ti.[23] The transfer technique of the MoS_2 flake is carried out to fabricate MoS_2 on metal contacts, as shown in Figure 1b. The current depends non-linearly on voltage and is almost symmetric under positive and negative bias, as shown in Figure 1e, indicating that Schottky contact has been formed between MoS_2 and Ti. The transfer technique of the MoS_2 flake is low energy so that the original perfect interface of MoS_2 and Ti is maintained.[24] In Figure 1c, the contacts of MoS_2 on and below Ti electrodes are formed with above-mentioned processes, respectively. The strong rectification is achieved in the current-voltage characteristics, as shown in Figure 1f, indicating that a lateral MoS_2 Schottky diode is prepared with different contact forms.

In order to further improve rectification ratio and lower dark current, higher Schottky barrier height is preferred. We choose Au as bottom electrode to contact with MoS_2 to expect high Schottky barrier height considering its larger work function. Ti continues to be selected to form ohmic contact. Unless otherwise specified, all contacts in this paper will be ohmic by magnetron sputtering deposition Ti on MoS_2. Because the Schottky contact is formed for MoS_2 on metals, we call it as MoS_2-on-metal Schottky photodetector. The 3D schematic and optical microscope diagram of the MoS_2 Schottky photodetector are shown in **Figure 2**a,b, respectively. The MoS_2 flake is transferred on the top of Au electrode, in which infrared light can penetrate through the MoS_2 flake to reach the contact interface for completely being absorbed by Au electrode, in contrast to the shadow of electrode on MoS_2 flakes. This results in improvement of efficiency of internal photoemission. The thickness of the MoS_2 flake we chose is 10 nm, corresponding to 15 monolayers, as shown in Figure 2c. The interval of Raman characteristic peaks between E^1_{2g} and A_{1g} is about 25 cm^{-1}, as shown in Figure 2(d), indicating that the MoS_2 flake is more than six layers, in agreement with atomic force microscopy measurement.[25]

The current–voltage characteristics of lateral MoS_2-on-Au Schottky photodetector measured in dark are shown in **Figure 3**a and the inset (semi-logarithmic coordinate). The strong rectification characteristic is obtained with rectification ratio of 10^3 at ±0.8 V. The dark current is about 1.2×10^{-10} A at –0.5 V bias voltage due to the large Schottky barrier. The ideal factor and Schottky barrier height can be extracted with the current–voltage characteristic curve.

The ideal factor (n) is described as[26]

$$n = \frac{q}{k \cdot T \cdot S \cdot \mathrm{In}(10)} \tag{1}$$

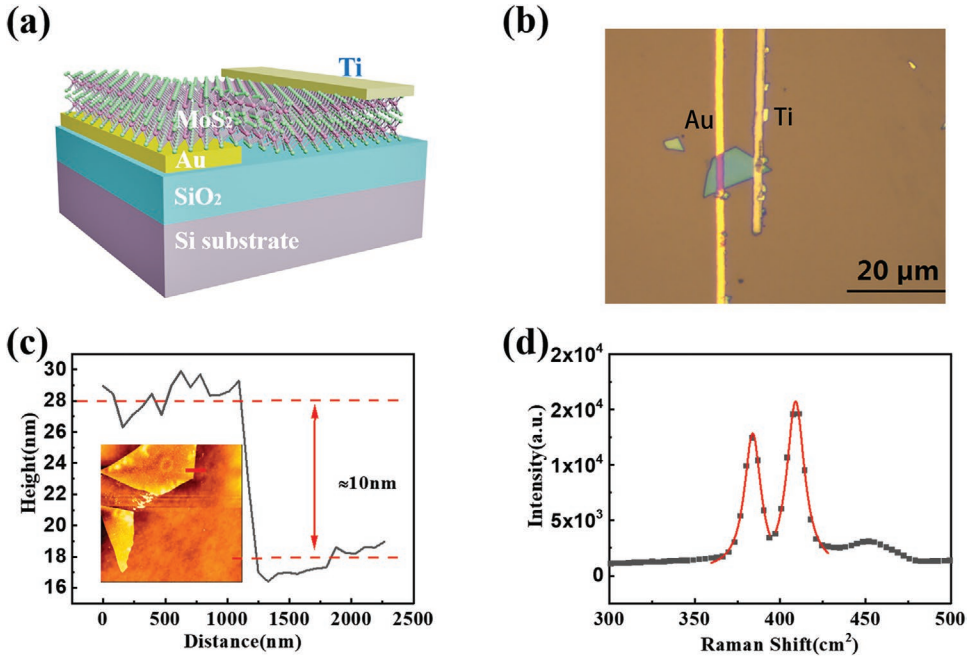

Figure 2. a) The 3D schematic view of the lateral MoS2 Schottky photodetector. b) Optical microscope diagram of MoS2-on-Au Schottky photodetector. c) The thickness of the MoS2 flake. The inset shows the AFM image of the MoS2 flake. d) The Raman spectra of the MoS2 flake.

where q is electron charge, k is Planck constant, T is temperature of 300 K and S is the slope of the linear region of the curve at forward bias voltage in semi-logarithmic coordinate. The Schottky barrier height (Φ_B) is described as[26,27]

$$\Phi_B = \left(\frac{k \cdot T}{q}\right) \mathrm{In}\left(\frac{A \cdot A^* \cdot T^2}{I_0}\right) \quad (2)$$

where A is the cross-sectional area of MoS_2 flake, A^* is Richardson constant of 54 A cm^{-1} K^{-2} for MoS_2,[28] I_0 is saturation current. The extracted ideal factor and effective Schottky barrier height are 1.55 and 0.53 eV, respectively. It is expected that the extracted Schottky barrier height should be higher than it actually is, due to the resistance of Van de Waals gap to the thermal electrons.

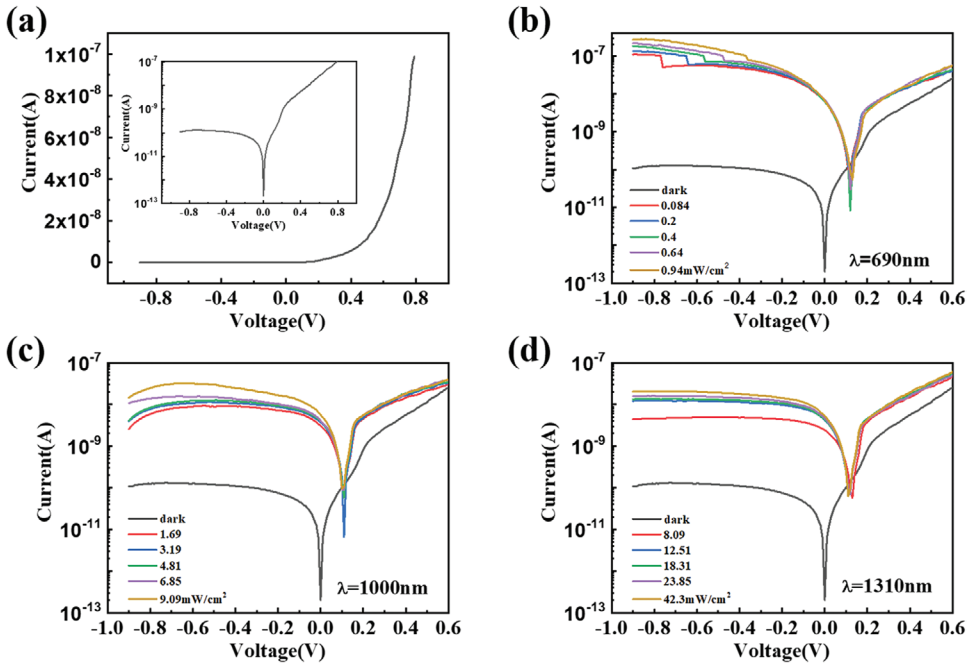

Figure 3. a) Dark current of MoS2-on-Au Schottky photodetector. The inset shows the dark current of (a) in semi-logarithmic coordinate. Variable power measurement of photoresponse of the MoS2-on-Au Schottky photodetector at b) 690 nm, c) 1000 nm, and d) 1310 nm.

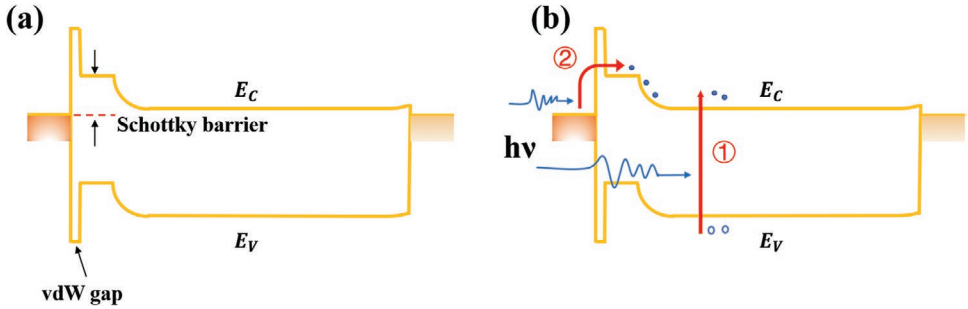

Figure 4. a) Band diagram of the MoS2-on-Au Schottky photodetector. b) Interband transition process and internal photoemission process in band diagram of the MoS2-on-Au Schottky photodetector.

Electrical characterization was repeated under various illumination intensities in the 0.084 to 0.94 mW cm^{-2} range at 690 nm, 1.69 to 9.09 mW cm^{-2} at 1000 nm, and 8.09 to 42.30 mW cm^{-2} at 1310 nm, as shown in Figure 3b,c,d respectively. The remarkable photoresponse was observed for the device at reverse bias and the photocurrent at reverse bias voltage increases monotonously with the increase of optical power. The ratio of photocurrent to dark current is about 10^3 for wavelength of 690 nm and 10^2 for the infrared region. Because the band gap of multilayer MoS_2 is about 1.3 eV, the cutoff wavelength due to interband transition is about 950 nm. The photoresponse at 690 nm can mainly be attributed to interband transition, as well as internal photoemission. Because the quantum efficiency of interband transition is much larger than that of internal photoemission and the light firstly penetrates into MoS_2, the carriers should be mainly generated in the MoS_2 multilayers to form large photocurrent. For the photoresponse with wavelength longer than 950 nm, the photoresponse mechanism cannot be attributed to the interband transition. Benefit from the structure of the Schottky junction formed by the MoS_2 located on Au electrode, the infrared light could penetrate through the MoS_2 flake to reach the contact interface and completely be absorbed by Au electrode to excite internal photoemission electrons into MoS_2 flakes.[18] It is worth noting that there is a significant zero shift of the current under illumination, which should be attributed to the built-in electric field of the Schottky junction. The remarkable photocurrent at zero bias indicates that the MoS_2 Schottky photodetector can be operated by self-powered in the range of visible and near-infrared wavelength.

The band diagram of the MoS_2 Schottky photodetector is shown in **Figure 4**a. MoS_2 on Au forms a Schottky barrier with a Van der Waals gap and Ti on MoS_2 flake is Ohmic contact. Due to Van der Waals gap, the band of MoS_2 only bends at the edge of the electrode and no electrons can directly tunnel through the Schottky barrier. The thermal electrons need to not only jump across the Schottky barrier but also tunnel through the Van der Waals gap to get into the semiconductor. Hence, the dark current is quite small and exhibits prominent Schottky characteristics. Figure 4b shows interband transition, marked as ①, and internal photoemission, marked as ②, processes in the MoS_2 on Au Schottky photodetectors under illumination. When light with wavelength shorter than 950 nm is illuminated into MoS_2, electrons in the valence band are excited by photons to the conduction band and electrons and holes are transported to electrodes to form photocurrent. When light with wavelength longer than 950 nm penetrates through the MoS_2 flake to reach the contact interface, the light-excited electrons in Au can jump across the barrier as well as tunneling through the Van de Waals gap into MoS_2 and collected by the Ti electrode. Due to the random direction of momentum of the excited electrons, the quantum efficiency of internal photoemission effects is always lower than that of interband transition by several orders of magnitude. If there are carrier traps in the MoS_2, the carrier lifetime is extended so that the high gain, as well as the high responsivity, can be obtained.[29–31] From the response spectrum shown in Figure S2, Supporting Information, it can be seen that the responsivity in the visible spectrum is as high as hundreds A W^{-1} and the responsivity in the near-infrared spectrum is about several A W^{-1}, which demonstrates the high photocurrent gain. Anyway, the responsivity in infrared spectrum is still high enough compared with those based on conventional semiconductors.[32] The difference in quantum efficiency between interband transition and internal photoemission should be responsible for the difference of responsivity in the visible or infrared spectrum.

Figure 5 shows responsivity and specific detectivity of the MoS_2 Schottky photodetector under different optical power at 690 nm. The specific detectivity (D^*) is extracted with the equation of[33,34]

$$D^* = \frac{\sqrt{A} \cdot R}{\sqrt{2qI_D}} \tag{3}$$

where A is the area of the device, R is the responsivity, q is electron charge, and I_D is the dark current. The responsivity and specific detectivity decrease with the increase of optical power. The maximum responsivity of 1252 A W^{-1} is obtained for the device at −0.5 V reverse bias voltage. The outstanding responsivity of 151 A W^{-1} and an amazing specific detectivity of 4.2×10^{14} Jones are achieved at zero bias voltage.

The responsivity and specific detectivity under different optical power at 1310 nm were measured, as shown in **Figure 6**a. Basically, the responsivity and specific detectivity decrease with the increase in the optical power, except the responsivity and detectivity at the minimum power. Maximum value of the responsivity at −1 V is 1.9 A W^{-1}, which corresponds to the specific detectivity of 2.3×10^{11} Jones. More importantly, the responsivity of 0.68 A W^{-1} and detectivity of 1.89×10^{12} Jones are extracted for the photodetector at zero bias voltage, which

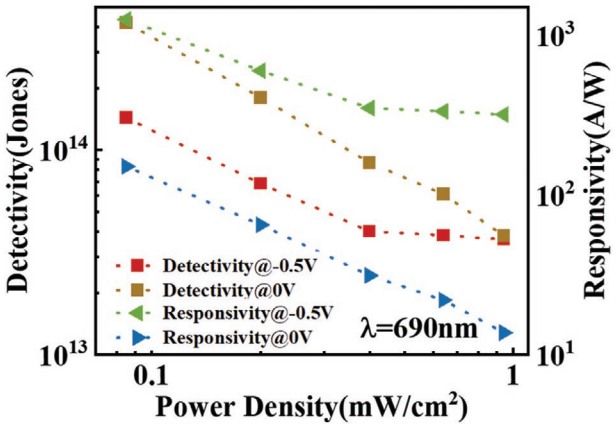

Figure 5. Responsivity and specific detectivity of the MoS2 Schottky photodetector under different optical power at 690 nm.

is comparable with interband transition mechanism dominated conventional semiconductor photodetectors for near-infrared operation. Those results demonstrate that the MoS_2 Schottky photodetectors can be operated by self-powered with high performance. Figure 6b shows the dependence of photocurrent of the MoS_2 photodetector under zero bias voltage on incident optical power at 1310 nm. The five test points in the Figure are fitted linearly to obtain the relationship: $I_{Ph} \propto P^{\alpha}$, where α is equal to 0.73, less than 1, indicating the existence of defects at the contact interface.

The high performance of self-powered MoS_2-on-Au Schottky photodetectors for near-infrared operation has been demonstrated thoroughly in terms of responsivity and specific detectivity at zero bias. In order to prove this method for fabrication of MoS_2 Schottky photodetector validation in general, electrical and photoresponse characterization of MoS_2-on-Ti Schottky diodes, as referred at the beginning, are also carried out. The optical microscope diagram of the device is shown in Figure S1c, Supporting Information. Raman spectroscopy and thickness measurement are shown in Figure S3, Supporting Information. **Figure 7**a shows the current–voltage characteristics and photocurrent of the MoS_2-on-Ti Schottky photodetector at 690, 1000, and 1310 nm, respectively. The dark current is about 10^{-10} A at –0.5 V reverse bias voltage and a rectification ratio of 10^2 at ±1 V is achieved. Similarly, the ideal factor of 3.1 and the effective Schottky barrier height of 0.51 eV were extracted from the dark current curves, respectively. The ideal factor is much larger than that in the MoS_2 on Au Schottky diode, implying more defects at the MoS_2–Ti interface. Compared to MoS_2-on-Au Schottky contact, the slight change in Schottky barrier height suggests that despite the existence of Van de Waals gap, Fermi level pinning effect still works. Under illumination of light at 690, 1000, and 1310 nm, the obvious photoresponse and zero shift in the bias voltage are observed. It is indicated that the stronger the photocurrent is, the larger the zero shift is in a certain range, regardless of wavelength. The zero shift is also observed in the variable optical power measurement at 1310 nm, as depicted in Figure 7b. The photocurrent significantly increases with the increase of incident power density and at zero bias remarkable photocurrent is observed, indicating the photodetector can work in self-powered mode. The responsivity and specific detectivity under different optical power at 1310 nm were shown in Figure 7c. The responsivity and detectivity increase with the increase of incident power density in the test range for the MoS_2-on-Ti Schottky photodetector under –0.5 V reverse bias, while decrease under zero bias. It is implied that external reverse bias enhances the electrical field at the Schottky junction and electron transportation. The built-in electrical field in the device at zero bias itself is not strong enough to transport the photoemission electrons under high incident power. On the other hand, lots of carrier traps at the MoS_2 on Ti interface may play an important role in this case. On the contrary, the responsivity of MoS_2 on Au Schottky photodetectors decreases with increase of incident power either at –0.5 V or 0 V bias, as shown in Figure 6a, indicating strong built-in electrical field at MoS_2 on Au interface and less effect of carrier traps.

The maximum value of responsivity of MoS_2-on-Ti Schottky photodetectors at –0.5 V reverse bias is about 66.2 mA W^{-1} at 1310 nm, which is much smaller than that of MoS_2-on-Au Schottky photodetectors. The responsivity and specific detectivity of MoS_2-on-Ti Schottky photodetectors at zero bias are about 19.2 mA W^{-1} and 1.09×10^{10} Jones.

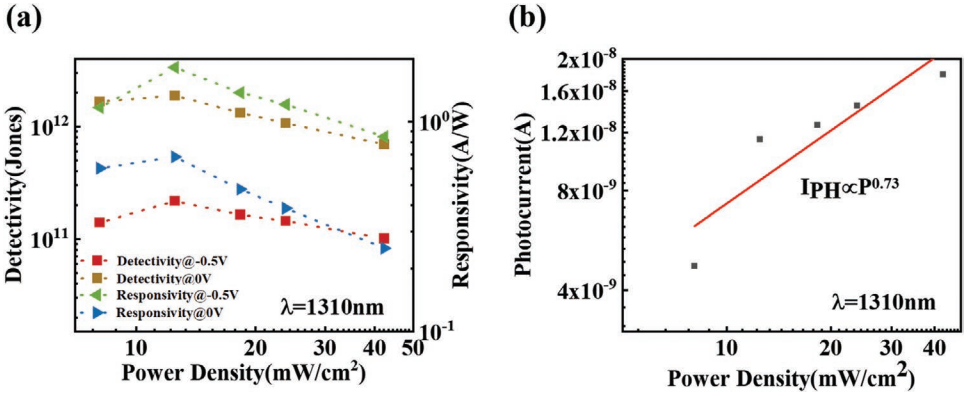

Figure 6. a) Responsivity and specific detectivity of the MoS2-on-Au Schottky photodetector under different optical power at 1310 nm. b) Dependence of photocurrent of the MoS2-on-Au Schottky photodetector on optical power density at 1310 nm.

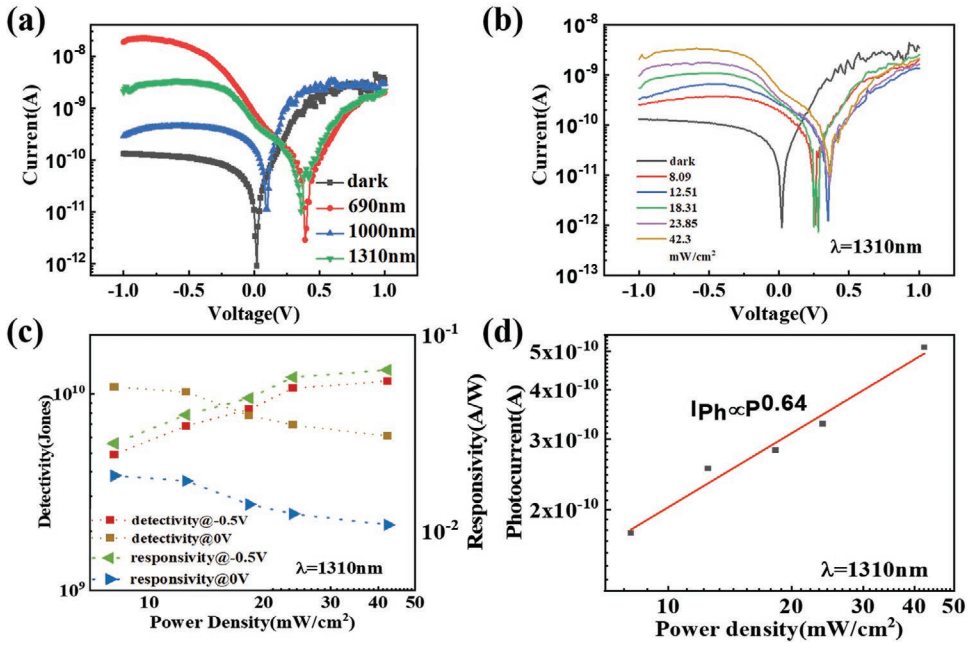

Figure 7. a) Photoresponse measurement of MoS2-on-Ti Schottky photodetector at 690, 1000, and 1310 nm. b) Variable optical power measurement of MoS2-on-Ti Schottky photodetector at 1310 nm. c) Responsivity and specific detectivity of the MoS2-on-Ti Schottky photodetector under different optical power at 1310 nm. d) Photocurrent of the MoS2-on-Ti Schottky photodetector at 1310 nm under different optical power.

The photocurrent of the MoS_2-on-Ti Schottky photodetector under variable optical power at 1310 nm is shown in Figure 7d. The dependence of photocurrent on optical power is fitted by the equation $I_{Ph} \propto P^{\alpha}$ with α of 0.64. The value of α is lower than that for the MoS_2-on-Au Schottky photodetector, also implying more defects at the MoS_2-Ti interface. In addition, variable power measurements of photoresponse are also performed at 690 and 1000 nm, as shown in Figure S4, Supporting Information. The responsivity and specific detectivity under different optical power at 690 and 1000 nm are shown in Figure S5, Supporting Information.

The large difference of device performance between MoS_2-on-Au and Ti may be attributed to the difference of photoemission efficiency of Au and Ti, defect or trap density at the MoS_2 and metal interface, built-in field of Schottky junction, as well as interface roughness. Anyway, Au or other metals with high work function may be more suitable for high-performance Schottky photodetectors with 2D materials in this method.

Table 1 lists the previously reported MoS_2 photodetectors operating at near-infrared wavelength for comparison. The maximum responsivity of 5.2 A W^{-1} at 1070 nm was achieved for the bilayer MoS_2 photodetector with hot electrons generated from plasmonic antenna array.[19] However, the large dark current and weak rectification property limit the overall performance of the devices. The MoS_2 vertical Schottky junction shows a low dark current of 10^{-12} A and good responsivity of 1 A W^{-1} at 1000 nm, near the cutoff wavelength of multilayer MoS_2, and fails to extend to longer wavelengths.[20] A broadband MoS_2 field-effect phototransistor with excellent photoresponse at 454 and 980 nm was achieved. However, due to the large dark current, available photoresponse characteristics were not realized at longer wavelength.[21] Very recently, the Au

Table 1. Comparison of Device Performance of MoS_2 based Photodetectors for near-infrared operation.

Device Materials	Operating wavelength [nm]	Responsivity [A W^{-1}]	Dark current [nA]	Detectivity [Jones]	Self-powered	Refs.
Au/MoS_2/Ti	1310	0.68@0V 1.9@-1V	≈10^{-4}@0V 0.12@-1V	1.89×10^{12} 2.3×10^{11}	Yes	This work
Au(RWs)/MoS_2/Au(NRWs)	1070	5.2@0.8V	≈10^{3}@3V		No	[19]
Au/MoS_2/ITO	1000	≈1@0V	≈10^{-3}@0V	≈10^{10}	Yes	[20]
Au/MoS_2/Au	980	2.3@0.2V	≈10^{3}@1V		No	[21]
Au/MoS_2(with Au NPs)/Au	980	0.064@15V	1.6@5V		No	[22]

We report a lateral self-powered MoS_2-on-metal Schottky photodetectors operating in the internal photoemission mode for near-infrared wavelength with high responsivity. In the MoS_2-on-Au Schottky photodetectors, the high responsivity of 0.68 A W^{-1} and the excellent specific detectivity of 1.89×10^{12} Jones at 1310 nm are obtained for the devices under 0 V.

nanoparticles decorated few-layer MoS_2 photodetector was proposed for operation at 980 nm, the responsivity was low, even at high bias voltage.[22] In this work, the responsivity of 0.68 A W^{-1} and detectivity of 1.89×10^{12} Jones at 1310 nm under 0 V bias are achieved, which is comparable with the performance of the photodetectors dominated by interband transition for near-infrared operation.

3. Conclusion

Self-powered MoS_2-on-metal Schottky photodetector with high responsivity and remarkable detectivity has been proposed and fabricated for near-infrared detection. The different contact forms of MoS_2 and metal fabricated by different processes show Schottky or Ohmic properties. With the MoS_2-on-Au Schottky photodetector operating in interband transition mode, the low dark current of 0.12 nA and high responsivity of 1252 A W^{-1} at −0.5 V reverse bias are achieved at 690 nm. The maximum responsivity of 1.9 A W^{-1} at 1310 nm is achieved for the MoS_2-on-Au Schottky photodetector operating in internal photoemission mode at −0.5 V bias. The high responsivity of 0.68 A W^{-1} and specific detectivity of 1.89×10^{12} Jones at 1310 nm are achieved for the photodetector at zero bias. The similar properties of MoS_2 on Ti contacts suggest that this simple method to fabricate Schottky photodetector with 2D material is in general to extend the photoresponse to infrared regions. The excellent performance of the self-powered MoS_2-on-Au Schottky photodetector for near-infrared operation provides the possibility for MoS_2 photodetector to work in the near-infrared photodetection and optical memory devices.

4. Experimental Section

Device Fabrication and Characterization: Heavily doped p-type Si substrate covered by 90 nm SiO_2 was cleaned by acetone, ethyl alcohol, and deionized water. Then, maskless laser direct lithography was carried out to define the pattern of electrode, followed by deposition of Au or Ti of 50 nm on the target substrate and lift-off to fabricate the bottom electrode. The MoS_2 flakes were mechanically exfoliated from bulk MoS_2 and transferred to a surface of 300 nm SiO_2 covering on a Si substrate. Then, a home-made alignment-transfer system was used to transfer the MoS_2 flakes on the metal electrodes to form Van der Waals contact. Firstly, through spinning polymethyl methacrylate (PMMA) on the Si substrate covered by 300 nm SiO_2 and etch of silicon dioxide layer in diluted hydrofluoric acid solution, the mechanically exfoliated MoS_2 flakes were separated from the initial substrate and held by the PMMA film. Then, the MoS_2 flakes held by the PMMA film were transferred onto polydimethylsiloxane (PDMS). After this step, the PMMA film was dissolved in hot acetone. Subsequently, the MoS_2 flake on PDMS was transferred on the substrate of premade bottom electrode and align with bottom electrode to form Van der Waals contact. After that, PMMA was spun on the surface of MoS_2 flake again followed by defining the pattern of the top electrodes by maskless laser direct lithography. Finally, 50 nm thick Ti was deposited on the sample by magnetron sputtering, followed by the lift-off process in 50 °C hot acetone to define the Ti electrodes. All devices were thermally annealed at 300 °C in vacuum for 2 h after fabrication. All the electrical and optoelectronic measurements were performed on the Keithley 2611B at room temperature. A Halide lamp was employed as a light source and a monochromator was used for splitting light.

Supporting Information

Supporting Information is available from the Wiley Online Library or from the author.

Acknowledgements

This work was supported by National Natural Science Foundation of China (Grant No. 62074134) and National Key Research Program of China (Grant No. 2018YFB2200103).

Conflict of Interest

The authors declare no conflict of interest.

Keywords

internal photoemission, MoS_2, near-infrared photodetection, Schottky photodetectors, self-powered electronics

Received: November 19, 2020
Revised: December 15, 2020
Published online: January 25, 2021

[1] J. Shim, H. Y. Park, D. H. Kang, J. O. Kim, S. H. Jo, Y. Park, J. H. Park, *Adv. Electron. Mater.* **2017**, *3*, 1600364.
[2] F. Schwierz, J. Pezoldt, R. Granzner, *Nanoscale* **2015**, *7*, 8261.
[3] Q. H. Wang, K. Kalantar-Zadeh, A. Kis, J. N. Coleman, M. S. Strano, *Nat. Nanotechnol.* **2012**, *7*, 699.
[4] K. F. Mak, J. Shan, *Nat. Photonics* **2016**, *10*, 216.
[5] C. Qin, Y. Gao, Z. Qiao, L. Xiao, S. Jia, *Adv. Opt. Mater.* **2016**, *4*, 1429.
[6] M. Luo, F. Wu, M. Long, X. Chen, *Nanotechnology* **2018**, *29*, 444001.
[7] W. Deng, Y. Chen, C. You, B. Liu, Y. Yang, G. Shen, S. Li, L. Sun, Y. Zhang, H. Yan, *Adv. Electron. Mater.* **2018**, *4*, 1800069.
[8] M. Dai, H. Chen, F. Wang, Y. Hu, S. Wei, J. Zhang, Z. Wang, T. Zhai, P. A. Hu, *ACS Nano* **2019**, *13*, 7291.
[9] S. Hu, Q. Zhang, X. Luo, X. Zhang, T. Wang, Y. Cheng, W. Jie, J. Zhao, T. Mei, X. Gan, *Nanoscale* **2020**, *12*, 4094.
[10] W. Choi, M. Y. Cho, A. Konar, J. H. Lee, G. B. Cha, S. C. Hong, S. Kim, J. Kim, D. Jena, J. Joo, S. Kim, *Adv. Mater.* **2012**, *24*, 5832.
[11] O. Lopez-Sanchez, D. Lembke, M. Kayci, A. Radenovic, A. Kis, *Nat. Nanotechnol.* **2013**, *8*, 497.
[12] X. Zhong, W. Zhou, Y. Peng, Y. Zhou, F. Zhou, Y. Yin, D. Tang, *RSC Adv.* **2015**, *5*, 45239.
[13] K. F. Mak, C. Lee, J. Hone, J. Shan, T. F. Heinz, *Phys. Rev. Lett.* **2010**, *105*, 136805.
[14] S. W. Han, H. Kwon, S. K. Kim, S. Ryu, W. S. Yun, D. H. Kim, J. H. Hwang, J. S. Kang, J. Baik, H. J. Shin, S. C. Hong, *Phys. Rev. B: Condens. Matter Mater. Phys.* **2011**, *84*, 045409.
[15] G. Eda, H. Yamaguchi, D. Voiry, T. Fujita, M. Chen, M. Chhowalla, *Nano Lett.* **2011**, *11*, 5111.
[16] Y. Deng, Z. Luo, N. J. Conrad, H. Liu, Y. Gong, S. Najmaei, P. M. Ajayan, J. Lou, X. Xu, P. D. Ye, *ACS Nano* **2014**, *8*, 8292.
[17] Y. Zhao, X. Xiao, Y. Huo, Y. Wang, T. Zhang, K. Jiang, J. Wang, S. Fan, Q. Li, *ACS Appl. Mater. Interfaces* **2017**, *9*, 18945.
[18] T. Hong, B. Chamlagain, S. Hu, S. M. Weiss, Z. Zhou, Y. Q. Xu, *ACS Nano* **2015**, *9*, 5357.

[19] W. Wang, A. Klots, D. Prasai, Y. Yang, K. I. Bolotin, J. Valentine, *Nano Lett.* **2015**, *15*, 7440.
[20] F. Gong, H. Fang, P. Wang, M. Su, Q. Li, J. C. Ho, X. Chen, W. Lu, L. Liao, J. Wang, W. Hu, *Nanotechnology* **2017**, *28*, 484002.
[21] J. Y. Wu, Y. T. Chun, S. Li, T. Zhang, J. Wang, P. K. Shrestha, D. Chu, *Adv. Mater.* **2018**, *30*, 1705880.
[22] J. Guo, S. Li, Z. He, Y. Li, Z. Lei, Y. Liu, W. Huang, T. Gong, Q. Ai, L. Mao, Y. He, Y. Ke, S. Zhou, B. Yu, *Appl. Surf. Sci.* **2019**, *483*, 1037.
[23] Y. Mao, A. Chang, P. Xu, C. Yu, W. Huang, S. Chen, Z. Wu, C. Li, *Semicond. Sci. Technol.* **2020**, *35*, 095023.
[24] J. Kang, W. Liu, K. Banerjee, *Appl. Phys. Lett.* **2014**, *104*, 093106.
[25] C. Lee, H. Yan, L. E. Brus, T. F. Heinz, J. Hone, S. Ryu, *ACS Nano* **2010**, *4*, 2695.
[26] S. M. Sze, K. K. Ng, *Physics of Semiconductor Devices*, Wiley, New York **2008**.
[27] V. Baranwal, S. Kumar, A. C. Pandey, D. Kanjilal, *J. Alloys Compd.* **2009**, *480*, 962.
[28] Neetika, S. K. , A. Sanger, H. K. Chourasiya, A. Kumar, K. Asokan, R. Chandra, V. K. Malik, *J. Alloys Compd.* **2019**, *797*, 582.
[29] M. M. Furchi, D. K. Polyushkin, A. Pospischil, T. Mueller, *Nano Lett.* **2014**, *14*, 6165.
[30] H. Fang, W. Hu, *Adv. Sci.* **2017**, *4*, 1700323.
[31] B. Miller, E. Parzinger, A. Vernickel, A. W. Holleitner, U. Wurstbauer, *Appl. Phys. Lett.* **2015**, *106*, 122103.
[32] J. Michel, J. Liu, L. C. Kimerling, *Nat. Photonics* **2010**, *4*, 527.
[33] G. Konstantatos, E. H. Sargent, *Nat. Nanotechnol.* **2010**, *5*, 391.
[34] J. Wang, H. Fang, X. Wang, X. Chen, W. Lu, W. Hu, *Small* **2017**, *13*, 1700894.